Journal of Power Sources 185 (2008) 40–48

Contents lists available at ScienceDirect

Journal of Power Sources

journal homepage: www.elsevier.com/locate/jpowsour

Nanoscale bismuth oxide impregnated (La,Sr)MnO_3 cathodes for intermediate-temperature solid oxide fuel cells

Zhiyi Jiang, Lei Zhang, Kai Feng, Changrong Xia*

Laboratory for Renewable Clean Energy, Department of Materials Science and Engineering, University of Science and Technology of China, Hefei, 230026 Anhui, China

ARTICLE INFO

Article history:
Received 29 June 2008
Accepted 3 July 2008
Available online 15 July 2008

Keywords:
Bismuth oxide
Solid oxide fuel cells
Impregnation
Impedance spectroscopy
Composite cathode

ABSTRACT

Bismuth oxide based oxygen ion conductors are incorporated into (La,Sr)MnO_3 (LSM), the classical cathode material for solid oxide fuel cells (SOFC), to improve the cathode performance. Yttria-stabilized bismuth oxide (YSB) is taken as an example and is impregnated into a preformed porous LSM frame, forming a highly active cathode for intermediate-temperature SOFCs (IT-SOFCs) with doped ceria electrolytes. X-ray diffraction indicates that YSB is chemically compatible with LSM at intermediate temperatures below 800 °C. The impregnated YSB particles are nanosized and are deposited on the surface of the framework. Significant performance improvement is achieved by introducing nanosized YSB into the LSM electrodes. At 600 °C, the interfacial polarization resistance under open-circuit conditions for electrodes impregnated with 50% YSB is only 1.3% of the original value for a pure LSM electrode. The resistance is further reduced dramatically when current is passed through. In addition, the YSB impregnated LSM electrodes has the highest electrochemical performance among those based on LSM. Single cell with 25% of YSB impregnated LSM cathode generates maximum power density of 300 mW cm^{-2} at 600 °C, indicating the promise of using LSM-based electrodes for IT-SOFC.

© 2008 Elsevier B.V. All rights reserved.

1. Introduction

Sr-doped lanthanum manganates $La_{1-x}Sr_xMnO_{3-\delta}$ (LSM) are the classical cathode materials for high-temperature solid oxide fuel cells (SOFCs) because of their good properties in electrical conductivity, catalytic activity for oxygen reduction, thermal and chemical stability in high temperatures, and compatibility with electrolytes such as yttria-stabilized zirconia (YSZ) and doped ceria (DCO). Unfortunately, LSM exhibits negligible ionic conductivities, and thus results in very poor electrochemical performance as the oxygen reduction is only able to occur at triple phase boundary (TPB) where oxygen ion conduction is possible. A general means for improving the performance is to add an ionic conductor into LSM to form a composite electrode, leading to a significant decrease in the interfacial polarization resistance. For instance, Murray and Barnett [1] reported that at 700 °C, the interfacial polarization resistance is 7.28 Ω cm^2 for pure LSM cathode, 2.49 Ω cm^2 for a LSM–YSZ composite cathode, and further dropped to 0.75 Ω cm^2 for a LSM–GDC (gadolinia-doped ceria) cathode. The resistance reduction associated with DCO addition is usually much larger than that with YSZ. This is because the oxygen ionic conductivity of DCO is about one order of magnitude higher than that of YSZ; in general, the higher the ionic conductivity is, the smaller the interfacial polarization resistance is.

Bismuth based oxides can be good electrolyte materials because of their high oxygen ionic conductivity [2]. The δ-phase Bi_2O_3 has 25% intrinsic oxygen vacancies, and thus results in oxygen ion conductivity that is about two orders of magnitude higher than that of yittria stabilized zirconia. The high-temperature δ-phase can be retained at lower temperatures by doping Bi_2O_3 with isovalent rare earth oxides such as yttria [3]. In addition, previous work showed that bismuth oxides had positive catalytic effects on oxygen dissociation process [4], which is often the rate-limiting step in oxygen reduction reaction at SOFC cathodes. Finally, under cathode atmosphere, doped bismuth oxides are expected be stable. Thus, stabilized bismuth oxides are promising for use as the ionic conducting phase for LSM-based electrodes. Further reduction in interfacial polarization resistance should be expected when bismuth oxides are used instead of ceria and zirconia based oxides.

Bismuth oxides have been previously used as the ionic conduction component in SOFC cathodes; in these applications, silver was often used as the electronic conduction phase [5,6]. As silver has a high thermal expansion coefficient of 19×10^{-6} K^{-1} [7], long term stability would be questionable for the composite cathodes con-

* Corresponding author. Tel.: +86 5513607475; fax: +86 5513606689.
E-mail address: xiacr@ustc.edu.cn (C. Xia).

0378-7753/$ – see front matter © 2008 Elsevier B.V. All rights reserved.
doi:10.1016/j.jpowsour.2008.07.003

sisting of silver and bismuth oxides. Since the thermal expansion coefficient of LSM matches that of common electrolytes such as YSZ and DCO, LSM seems to be a better choice. Recently, Li et al. [8] reported an $(La_{0.74}Bi_{0.10}Sr_{0.16})MnO_3$–$(Bi_2O_3)_{0.7}(Er_2O_3)_{0.3}$ composite cathode for zirconia based electrolytes. In this work, cathodes composed of LSM and yttria-stabilized bismuth oxides (YSB) are evaluated when Sm-doped ceria (SDC) is used as the electrolyte in both symmetrical and single cell configurations. Possible reaction between YSB and LSM is also investigated.

A possible drawback of using YSB as the cathode component is the thermal expansion coefficient mismatch. The thermal expansion coefficient is $14.6 \times 10^{-6}\,K^{-1}$ for YSB [9], which is higher than $\sim 11 \times 10^{-6}\,K^{-1}$ for DCO electrolytes, [10]. To mitigate this problem, in our present study, YSB is introduced with an ion impregnation process. In this process, YSB will be embedded in pre-formed LSM backbone. The effect of LSM and YSB firing temperature on the electrode performances will be also investigated for the purpose of optimizing the electrode performance.

2. Experimental procedures

2.1. Powder preparation

SDC ($Sm_{0.2}Ce_{0.8}O_{1.90}$), A-site nonstoichiometric LSM ($(La_{0.85}Sr_{0.15})_{0.9}MnO_{3-\delta}$), and YSB ($(Y_{0.25}Bi_{0.75})_2O_3$) powders were synthesized using a glycine-nitrate process [11]. All the starting chemicals were of analytical grade and from Sinopharm Chemical Reagent Co., Ltd. To synthesize SDC powders, stoichiometric amounts of $(NH_4)_2Ce(NO_3)_6$ and $Sm(NO_3)_3$ were dissolved in distilled water to form a mixed solution, to which glycine was added at a glycine to nitrate molar ratio of 0.5. The resulting solution was heated on a hot plate till self-combustion occurred, yielding a homogeneous yellowy powder, followed by firing at 600 °C for 2 h to remove possible glycine residues and meanwhile coarsen the powders. LSM powders were synthesized using $La(NO_3)_3$, $Sr(NO_3)_2$, and $Mn(NO_3)_2$ as starting chemicals. The raw powders were heated at 800 °C for 2 h to form LSM solid solution, which was confirmed to be perovskite structure by X-ray diffraction. YSB powders were prepared with $Y(NO_3)_3$ and $Bi(NO_3)_3$ as the precursors. The as-synthesized products were fired at 600 °C for 2 h to form cubic structured YSB solid state solutions. To investigate the chemical compatibility between the two materials, LSM and YSB powders were mixed at a 1:1 weight ratio, pressed to discs and then fired at 900 °C for 12 h.

2.2. Cell fabrications

Symmetrical cells were constructed with SDC electrolyte substrates and porous LSM framework loaded with YSB nanoparticles. The substrates were prepared by cold-pressing and subsequently sintering SDC powders at 1400 °C for 5 h. The sintered substrates were about 13 mm in diameter and 0.7 mm thick. LSM frameworks were prepared using a screen printing technique. A LSM slurry was prepared by mechanically mixing LSM powders with organic additives such as terpilenol. The porous LSM networks with thickness of about 50 μm were obtained by screen-printing of the slurry onto both sides of the substrates, followed by drying with an infrared lamp, and firing at 900 °C for 2 h. The porosity was estimated to be 60% with the thickness and weight of the network. The samples were also fired at 800 °C and 1000 °C to investigate the effect of firing temperature on the electrode performance. YSB was then introduced into the porous networks with an ion impregnation method [12]. The impregnation process was conducted as follows. A solution containing 25 mol% $Y(NO_3)_3$ and 75 mol% $Bi(NO_3)_3$ was infiltrated into the porous networks; the infiltrated sample was dried at room temperature, and heated at 800 °C for 2 h to convert the nitrates into YSB nanoparticles. The impregnated products were also heated at 650, 700, 750, and 850 °C to find out the optimal fabrication temperature. The cells were weighed before and after each impregnation-and-heating cycle to determine the loading of the impregnated YSB (X_{YSB}) which is defined as the weight percent of YSB in the electrode.

$$X_{YSB} = \frac{w_{YSB}}{w_{YSB} + w_{LSM}} \times 100\% \quad (1)$$

where w_{YSB} was the weight of impregnated YSB and w_{LSM} was the weight of the porous network.

Anode-supported single cells with SDC as the electrolytes and Ni-SDC as the anodes were fabricated with a co-pressing and co-firing method [13]. Mixed powders of NiO, SDC and starch (60:40:20 wt.%) were pressed to form green substrates, on which SDC powders were co-pressed to form bilayer structures. The bilayers were subsequently co-fired at 1250 °C for 5 h to densify the electrolyte layers. Cathodes were fabricated on the electrolytes with the same process as that for the symmetrical cells. The cathode area was about 0.5 cm^2.

Three-electrode half cells were also fabricated to study the activation effect of current on the electrode performance. Pt counter electrode was located symmetrically to the YSB impregnated LSM working electrode, at the center of the opposite side of the electrolyte. The ring-shaped Pt reference electrode was around the working electrode. The configurations of the symmetrical cell, single cell, and three-electrode half cell were illustrated in Fig. 1.

2.3. Characterizations

Phase structure was identified with X-ray diffraction technique (XRD, Philips X'pert PROS diffractmeter). Morphology and microstructure were observed by scanning electron microscopy (SEM, FEI XL30). Electrochemical measurements were conducted with a Zahner Im6ex electrochemical workstation. Ag paste and Ag wires were used to ensure the electronic contact. The impedance of a symmetric cell was measured in ambient air, and typically in the frequency range of 3 MHz to 0.1 Hz with signal amplitude of 10 mV over a temperature range 550–800 °C. The furnace temperature was controlled with a thermal couple close to the sample. The spectra were fitted using an analysis software (ZSimpWin, PerkinElmer Instruments). Area specific interfacial polarization resistance, R_p, was determined by the difference of the low and high frequency intercepts at the real axis. Single cell performance was tested while humidified (3% H_2O) hydrogen was fed at a flow rate of 60 ml min^{-1} as the fuel and ambient air as the oxidant. All impedance spectra for single cells were recorded under open-circuit conditions with 10 mV perturbation.

3. Results and discussion

3.1. Cathode composition and microstructure

Shown in Fig. 2 are the XRD patterns of LSM powder fired at 900 °C for 2 h, YSB powder fired at 600 °C for 2 h, LSM–YSB composite prepared by mechanically mixing the YSB and LSM powders and heating the oxide mixture at 900 °C for 12 h, and LSM impregnated with 40% YSB, which was fired at 800 °C for 2 h. YSB and LSM solid solutions are formed with cubic (JPCDS PDF #84–1450) and perovskite structure [14], respectively. The XRD peaks of the composite powder can be ascribed to the cubic phase of YSB and perovskite phase of LSM without any other unexpected phases. This suggests that there is no obvious reaction between LSM and YSB

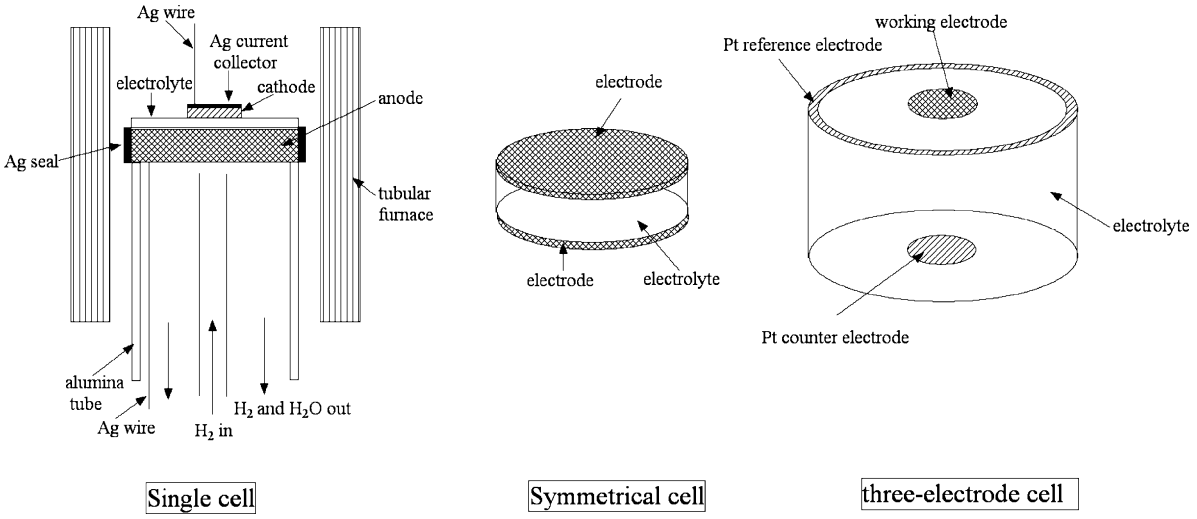

Fig. 1. Schematic configurations of the symmetric cell, single cell, and three-electrode cell.

even though they were mixed and fired at 900 °C for 12 h. Therefore, YSB and LSM are chemically stable under the SOFC operating conditions, i.e., at intermediate temperatures below 750 °C. XRD pattern also shows that cubic YSB was formed when the impregnated product was heated at 800 °C. The crystalline size estimated with Scherrer Equation [11] was about 27 nm, indicating that the impregnated particles were very fine even it was fired at 800 °C. For a comparison, the particle size of YSB fired at 600 °C was estimated to be 45 nm when it was prepared with the glycine-nitrate process.

Shown in Fig. 3 are the typical cross-sectional SEM images of the LSM networks impregnated with different amounts of YSB. As shown in Fig. 3a, the microstructure shows a porous character of the screen-printed LSM layer fired at 900 °C for 2 h. The LSM particles are porous, and exhibit irregular shapes with a few micrometers in size, and are sintered together forming a porous network structure. When the network was impregnated with YSB, the porosity decreased progressively. As shown in Fig. 3b, when 20% YSB is impregnated, the LSM particles are partially covered with YSB particles. The profile of micro-sized LSM particles could be clearly seen, and spherical YSB particles and clusters are isolated on the surface of the LSM particles. The YSB particles are at the nanoscale and their sizes can be as small as 10 nm. This is consistent with that estimated with the XRD pattern. When 40% YSB embedded into the porous network, the profile of LSM disappeared, only a continuous structure formed by the connection of YSB particles could be seen (Fig. 3c). It is reasonable that as the YSB loading increased, the YSB microstructure in the cathode would evolve from isolated particles (or clusters) to a layer of consecutively connected YSB particles. The microstructural characteristics are very similar to that of LSM cathodes impregnated with DCO electrolytes [12]. Fig. 3d gives the view of physical interface between an SDC electrolyte and an YSB impregnated LSM electrode. The adhesion of the electrolyte and electrode was greatly enhanced by introducing the YSB particles at the interface. Moreover, in the latter section it will be discussed that the presence of YSB at the interface was favorable for reducing the interface polarization resistance.

3.2. Impedance spectra for symmetrical cells

Electrodes with less than 50% of YSB loading were fabricated and investigated. A cathode with higher than 50% of YSB loading was not prepared because at such a high loading, the impregnation process became very difficult due to a very small porosity of the electrode. The porosity was estimated to be 32% when the loading was 50%. In addition, the electrode performance would become worse when its porosity was too low due to concentration polarization. Impedance spectra for LSM electrodes with various loadings were measured with a symmetrical cell configuration. The shape of the impedance spectra of YSB impregnated LSM electrode was similar to that of other LSM-based composite cathodes, such as LSM–YSZ [15], LSM–GDC [14], and DCO impregnated LSM [12]. In the testing temperature range, the impedance spectra of pure LSM electrode presented three arcs, whereas YSB impregnated LSM electrodes exhibited two or three arcs in their spectra, depending on the testing temperature. Although there are discrepancies on the mechanism for O_2 reduction on LSM-based electrodes, it is generally accepted that the O_2 reduction is controlled by O^{2-} migration at the electrode–electrolyte interface, oxygen adsorption and dissociation, oxygen surface diffusion, and gas diffusion [15–18]. The arc presented at different frequencies corresponded to these controlling steps. To identify these steps, equivalent circuit, $LR_0(R_1\mathrm{CPE}_1)(R_2\mathrm{CPE}_2)$ and $LR_0(R_1\mathrm{CPE}_1)(R_2\mathrm{CPE}_2)(R_3\mathrm{CPE}_3)$ (Fig. 4d) was applied to fit the impedance spectra recorded at different temperatures using ZsimpWin program. In the circuit, L is the

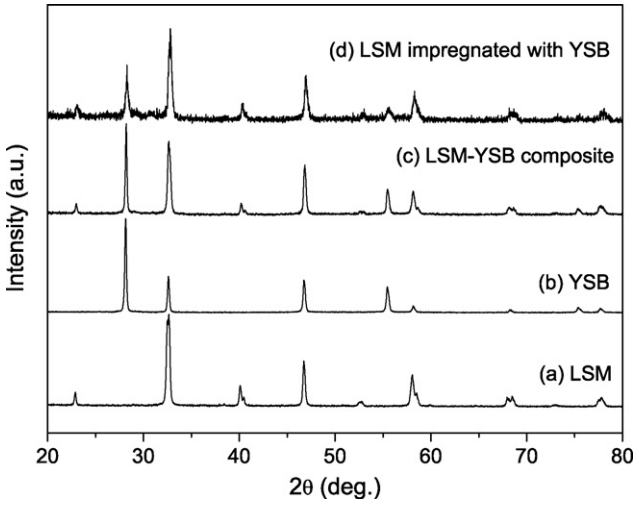

Fig. 2. XRD patterns of (a) LSM fired at 900 °C for 2 h, (b) YSB fired at 600 °C for 2 h, (c) a mixture of YSB and LSM (1:1 weight ratio) fired at 900 °C for 12 h, and (d) LSM impregnated with 40% YSB, which was fired at 800 °C for 2 h.

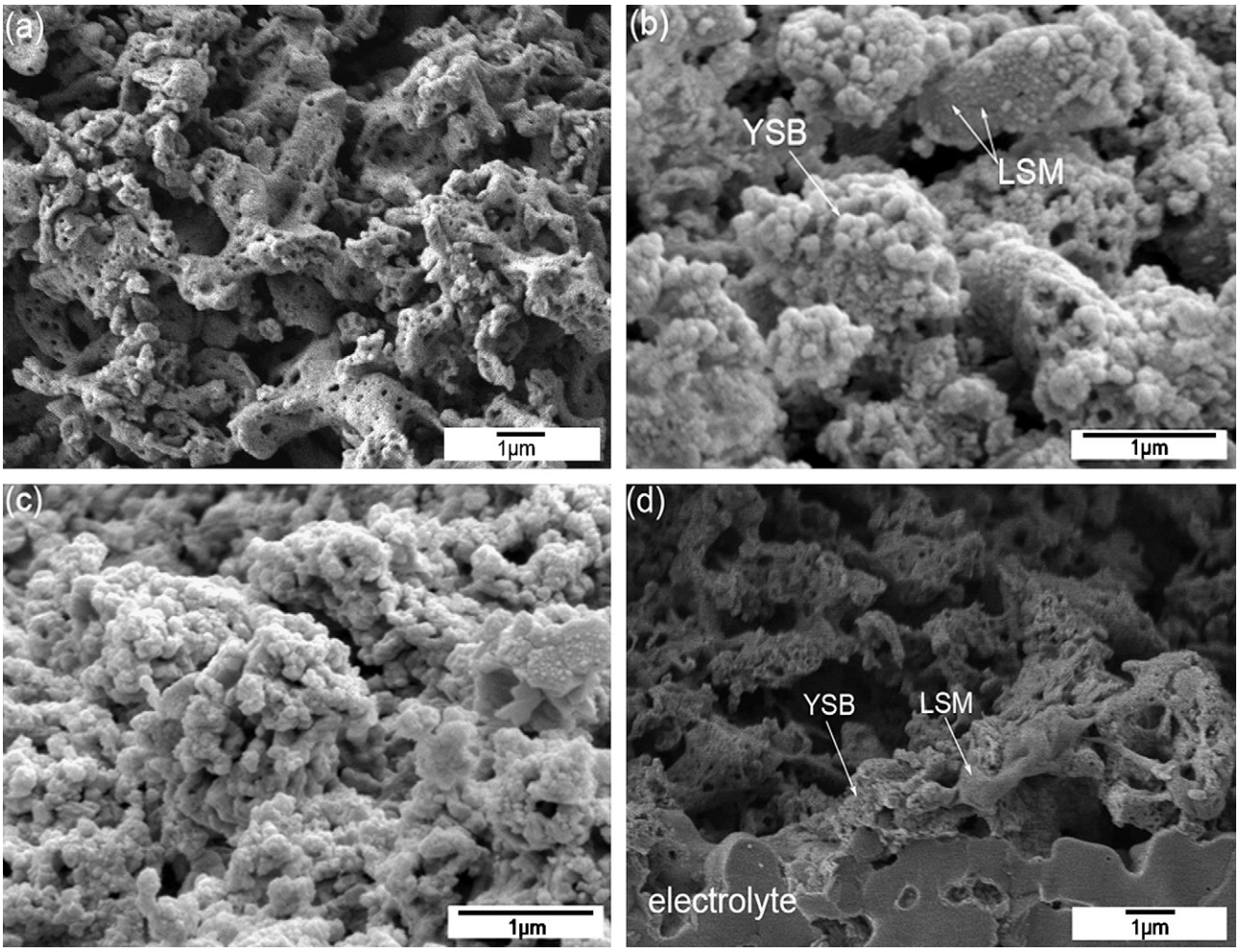

Fig. 3. Cross-sectional micrographs of (a) a pure LSM cathode, (b) a 20% YSB impregnated LSM cathode, (c) a 40% YSB impregnated LSM cathode, and (d) the interface between SDC electrolyte and 40% YSB impregnated LSM cathode. LSM was fired at 900 °C for 2 h and YSB was fired at 800 °C for 2 h.

inductance arising from the apparatus, R_0 is attributed to the resistance of electrolyte and lead wires, and $(R_n\text{CPE}_n)$ is the equivalent circuit for each electrochemical process identified at different frequency range, where R_n is the corresponding polarization resistance, and CPE_n is the corresponding constant phase element. The expression of CPE (often noted as Q) is $\text{CPE} = Y_0(jw)^n$, where Y_0 is the admittance, w is the angular frequency, and n is an exponent ($0 < n < 1$). It should be noted that in this study $(R_1\text{CPE}_1)$, $(R_2\text{CPE}_2)$, and $(R_3\text{CPE}_3)$ represent the high, intermediate frequency, and low frequency arc, respectively. As an example, Fig. 4 shows the spectra of electrodes loaded with 0% (pure LSM), 20% and 50% YSB, measured at 700 °C. The influence of YSB impregnation is clearly characterized by reduction of spectra scale and by the difference of spectra shape, and is discussed in detail as follows.

The effect of YSB loading on the resistance of the high frequency arc is illustrated in Fig. 5a, the Arrhenius plots of $1/R_1$ with various YSB loading. The activation energy of $1/R_1$ for electrodes with different YSB loading were ~1.1 eV, which is close to ~1 eV for the oxygen conduction in SDC [19] and in YSB [20], and this was consistent with that the high frequency response for LSM-based electrode, which is usually related to O^{2-} incorporation into electrolyte from TPB, and transport in the electrolyte component in the electrode [15–18]. The value of $1/R_1$ increases with the loading, suggesting a positive effect of YSB on the electrochemical process. As can be seen from the SEM image, fine YSB particles enhance the bonding between the electrode and electrolyte, Consequently, O^{2-} incorporation process is accelerated by the presence of YSB at the interface. And a high incorporation rate is expected at high loading. Another evidence for the increased O^{2-} incorporation rate is the calculated pseudo capacitance C_1 of $R_1\text{CPE}_1$. For the pure LSM electrode, the corresponding pseudo capacitance, C_1, was about 3 μF cm^{-2} at temperatures in range of 600–700 °C. When 20% YSB was loaded, it increased by a factor of 10 to about 30 μF cm^{-2}. It further increased to ~3000 μF cm^{-2} when 50% YSB was impregnated. As this high frequency process directly links with the TPB, larger capacitance indicates larger TPB area, and larger TPB area means more parallel O^{2-} incorporation paths. Higher YSB loading gives higher coverage level, resulting in more TPB sites.

Fig. 5b shows the Arrhenius plots of $1/R_2$. The effect of YSB loading on R_2 is similar to that on R_1; higher YSB loading results in smaller resistance and larger capacitance. The activation energy of $1/R_2$ for electrodes with different YSB loading was close to each other and over a range 1.3–1.5 eV, which was similar to those reported by Murray et al. for LSM–GDC [1] and LSM–YSZ [14]. This process is characterized by a relative high value of n for the constant phase element, which is about 0.8, the same as reported by Murray [15]. Generally, the intermediate frequency arc is attributed to oxygen adsorption and dissociation processes on the electrode surface [1,15,17,18]. Almost the same n value was observed for LSM electrodes with and without YSB, indicating that the presence of

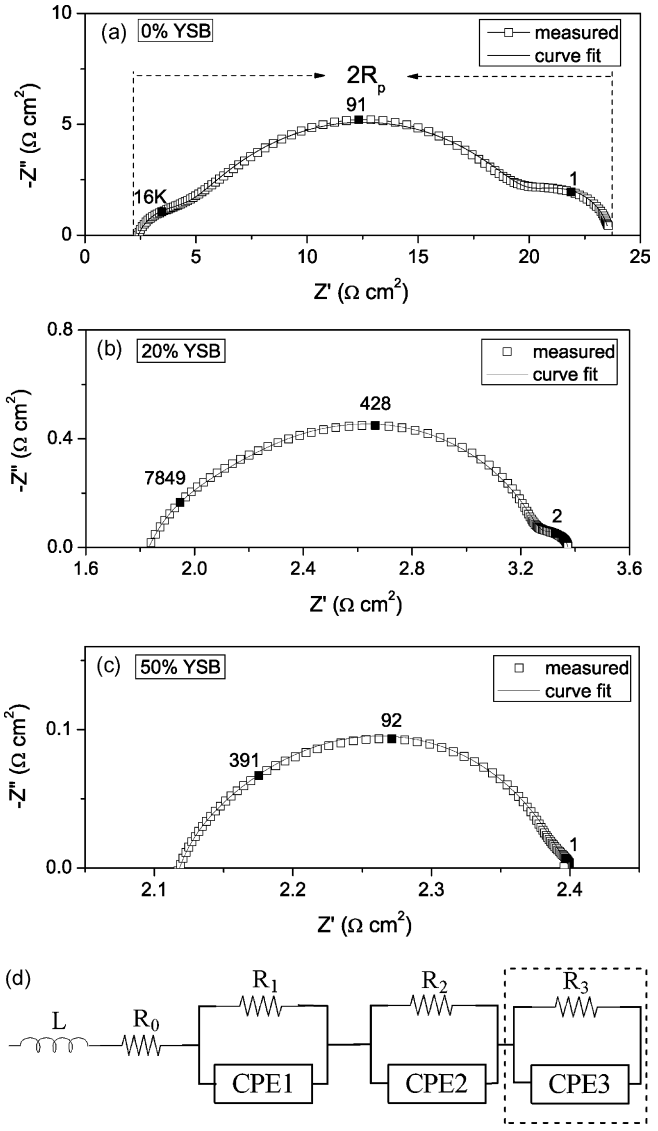

Fig. 4. Impedance spectra at 700 °C for LSM electrodes impregnated with (a) 0% (without impregnation), (b) 20%, and (c) 50% YSB. Subpart (d) shows the equivalent circuit used for fitting the spectra. Specific frequencies for each process are also illustrated.

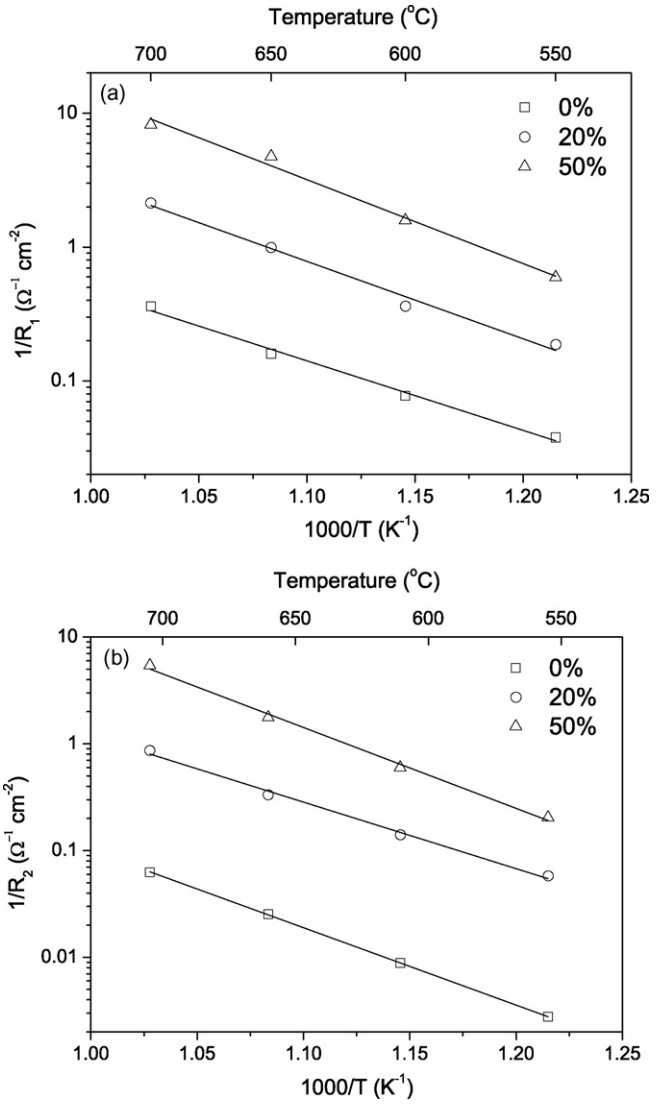

Fig. 5. Arrhenius plots for (a) $1/R_1$ and (b) $1/R_2$ determined from equivalent circuit fitting analysis of impedance spectra for LSM electrodes with various YSB loading.

YSB accelerates the oxygen adsorption and dissociation processes without changing the mechanism. The dependence of R_2 and capacitance on YSB loading was related to the catalytic activity of YSB associated with oxygen dissociation [4]. More YSB was impregnated, more oxygen dissociation sites were created, resulting in smaller resistance and larger capacitance.

A low frequency arc (Fig. 4a) was present in our testing temperature range for the pure LSM electrode and at temperature higher than 650 °C for the impregnated electrodes. The value of n of the low frequency arc was close to 1 for the LSM electrodes with and without YSB impregnation. Therefore, a pure capacitance behavior is expected for the process corresponding to the low frequency arc. The process is usually attributed to surface diffusion of oxygen species and/or gas diffusion. But the arc for pure LSM and YSB impregnated LSM could not be attributed to the same process because the arc for YSB impregnated LSM was observed only at high temperatures whereas the arc for pure LSM was present at all temperatures. The arc for pure LSM might be attributed to surface diffusion of oxygen species as reported by different authors regarding LSM-based electrodes [12,15,17]. Firstly, the porosity of pure LSM electrode was high enough, i.e., about 60%, and oxygen reduction process on pure LSM electrode is generally very low. Secondly, this arc was present at temperatures as low as 550 °C. And at such low temperatures, the LSM electrode process is further slowed down. Finally, the activation energy for this process was 1.51 eV, and the rate of gas diffusion shows weakly dependence on the temperature [21,22]. When LSM was impregnated with YSB, the arc disappeared at low temperatures. The absence of this arc was possibly because that the impregnated YSB extended the TPB and shortened the pathway for surface diffusion. An additional low frequency arc emerged, however, at temperatures higher than 650 °C, and the resistance for this arc had a weak dependence on temperature; for example, the resistance is 0.09 Ω cm^2 and 0.08 Ω cm^2 at 750 °C and 800 °C, respectively, for the electrode with 20% YSB loading. As mentioned above, impregnating YSB would decrease the porosity of the electrode. Thus, this arc was probably ascribed to gas diffusion in the electrode, which commonly acts as the rate-limiting step at high temperatures for composite electrodes [16].

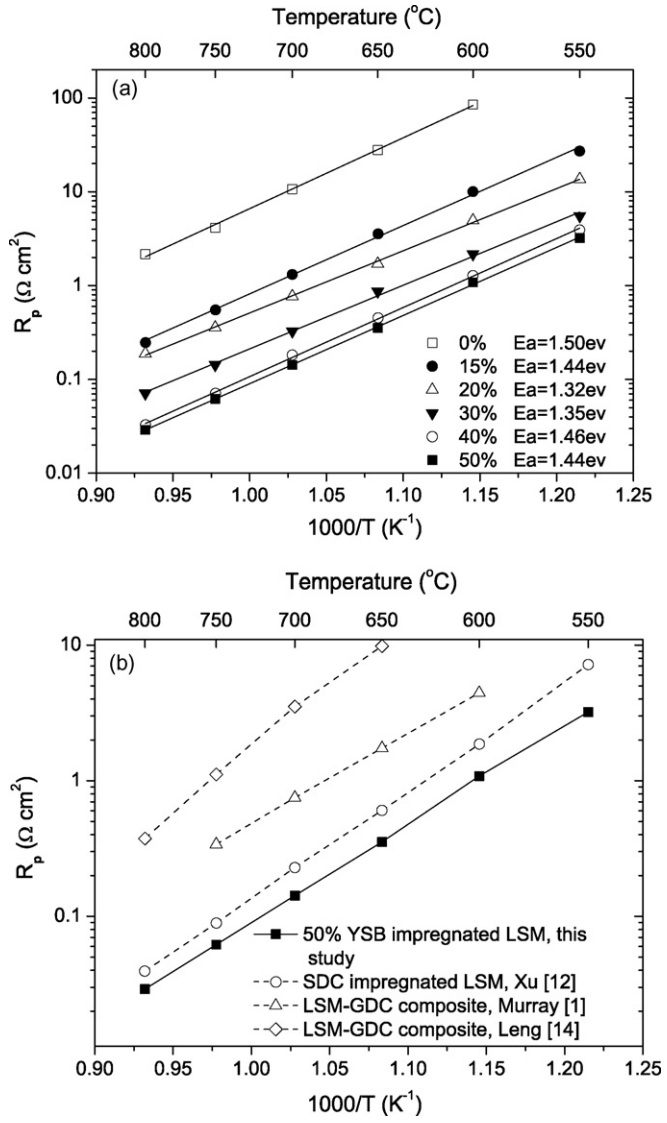

Fig. 6. (a) Temperature dependence of area specific polarization resistance, R_p for the interfaces between SDC electrolytes and LSM electrodes with various YSB loading, (b) comparison of the resistance for LSM-based cathodes with doped ceria as the electrolytes.

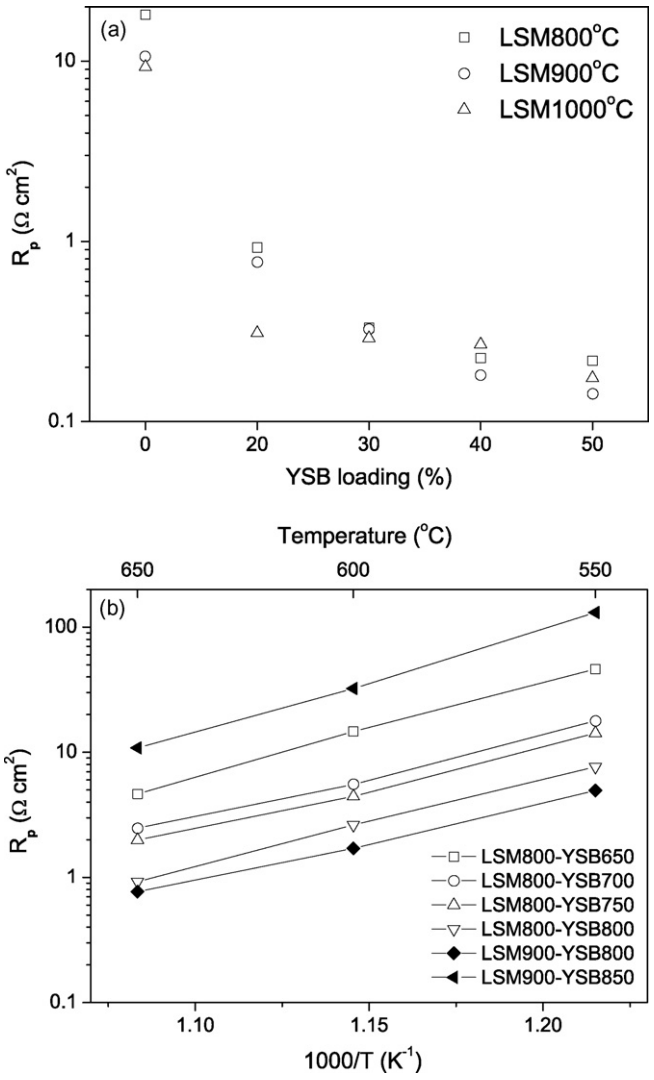

Fig. 7. (a) Area specific polarization resistance, R_p, at 700 °C for cells with LSM fired at 800 °C, 900 °C, and 1000 °C. The YSB heating temperature was 800 °C, (b) comparison of R_p for cells with YSB heated at 650 °C, 700 °C, 750 °C, 800 °C, and 850 °C. The LSM firing temperature was 800 °C and 900 °C, and the YSB loading was 20%.

3.3. Interfacial polarization resistances of symmetrical cells

Shown in Fig. 6a is the effect of YSB loading on area specific interfacial polarization resistance, R_p, for LSM electrodes on SDC electrolytes. The apparent activation energy for the resistance is also shown. R_p is half of the difference between the real axis intercepts of the impedance arcs, $R_p = (R_1 + R_2 + R_3)/2$. In the range of 0–50% YSB, higher loading resulted in smaller resistance. R_p of pure LSM electrode at 600 °C was 85.2 Ω cm^2. It decreased to 4.95 Ω cm^2 when 20% YSB was impregnated, and further to 1.08 Ω cm^2, only 1.3% of the original value, when 50% YSB was loaded. The electrode performance is substantially improved by incorporating YSB into LSM electrodes. As discussed above, fine YSB particles deposited on the surface of LSM particles would significantly extend the triple phase boundaries for O_2 reduction, resulting in a decrease in R_p. The performance would be significantly enhanced even at relative low YSB loadings. Although at low loadings the impregnated YSB particles are isolated (Fig. 3b), YSB particles fill the holes at the electrolyte/electrode interface thereby enhancing the bonding between the electrolyte and electrode, meanwhile extending the TPBs at the physical electrolyte/electrode interface. As the loading increases, the YSB particles gradually form a continuous coverage on the LSM particles, extending the TPBs from the physical cathode/electrolyte interface to the bulk of cathode. It can be seen from Fig. 6a that the slope of curves in the Arrhenius plots of all the cathodes seems to be very close. For pure LSM, the apparent activation energy was 1.50 eV, and that of LSM–YSB composite cathodes varied from 1.32 eV to 1.46 eV. YSB loading has little effect on the apparent activation energy, suggesting that introducing YSB into the LSM cathode does not significantly change the mechanism of oxygen reduction.

The performance of LSM-based electrodes is affected by both the fabrication process and the electrolyte component that is used to increase their activity. Shown in Fig. 6b is R_p comparison for LSM-based cathodes where doped ceria was used as the electrolytes. LSM impregnated with YSB shows the lowest R_p among LSM-based cathodes including LSM–GDC (gadolinia-doped ceria) [1,14] and LSM–SDC [12], which were prepared with different methods such as slurry printing [1] and ion impregnation [12,14]. The better performance of YSB impregnated LSM can be explained, at least in part,

by the high conductivity of YSB. For example, at 700 °C, the high frequency impedance for LSM impregnated with 20% YSB has similar pseudo capacitance with that impregnated with 25% SDC. Both of the values are 4×10^{-5} F cm^{-2}, but the resistance, R_1 is 0.47 Ω cm^2 for YSB impregnated LSM, which is smaller than that for the SDC impregnated one, 0.61 Ω cm^2. The oxygen ionic conductivity at 700 °C is 0.189 S cm^{-1} for YSB [23] while it is 0.041 S cm^{-1} for SDC [24]. High ionic conductivity will, as discussed above, reduce the high frequency arc. Although the influence on the high frequency arc is not the whole story for the influence of the ionic conductivity on the oxygen reduction, however, this process is directly linking with the ionic conductivity of the electrolyte and ionic phase in the electrode. Meanwhile, the higher conductivity of YSB allows the effective TPBs to extend more deeply into the bulk of cathode, in other words, more effective sites for O_2 reduction are available. It should be noted that, as mentioned above, YSB is a favorable catalyst for oxygen dissociation [4], which might also contribute to the high cathode performance.

3.4. Effect of LSM and YSB firing temperature

Shown in Fig. 7a is effect of LSM firing temperature on the electrode performance measured at 700 °C. For pure LSM electrodes, R_p decreased with firing temperature, which was below 1000 °C in this work. High firing temperature is often believed to enhance the bonding between the electrolyte and LSM. The same tendency was observed when LSM was impregnated with a small amount of YSB. However, when 30% YSB was loaded, R_p did not change much with LSM firing temperature. This infers that impregnated YSB gradually enhance the bonding between the electrode and electrolyte. When the loading exceeded 30%, electrodes with LSM fired at 900 °C showed the lowest R_p. When the YSB loading was high enough, the YSB particles would connect to each other forming an ionic pathway throughout the electrode, extending the TPBs into the whole electrode bulk. But, YSB filler would reduce the porosity of the electrode. Accordingly, as YSB loading was increased to 40% and 50%, an electrode with LSM fired at 900 °C would possess a microstructure that can balance its porosity and adhesion between electrode and electrolyte, leading to the lowest R_p.

Shown in Fig. 7b is the R_p dependence on YSB heating temperature. LSM firing temperature was 800 °C, and 20% YSB was impregnated. R_p decreased as heating temperature was raised from 650 °C to 800 °C; but it increased significantly when YSB was heated at 850 °C. XRD analysis showed there was not obvious composition

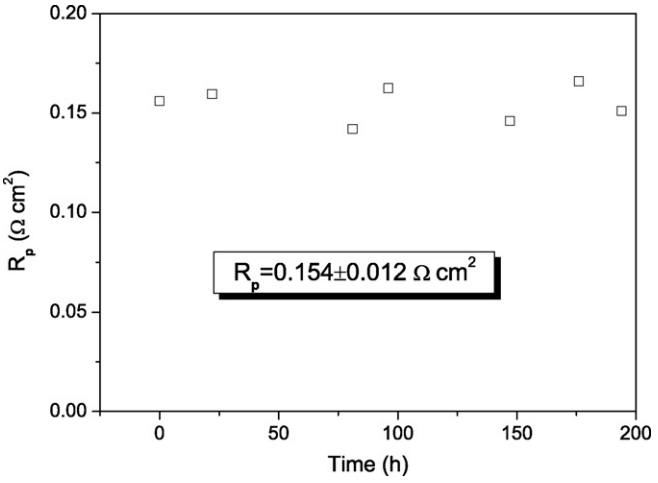

Fig. 8. R_p vs. time for 40% YSB impregnated LSM electrode at 700 °C.

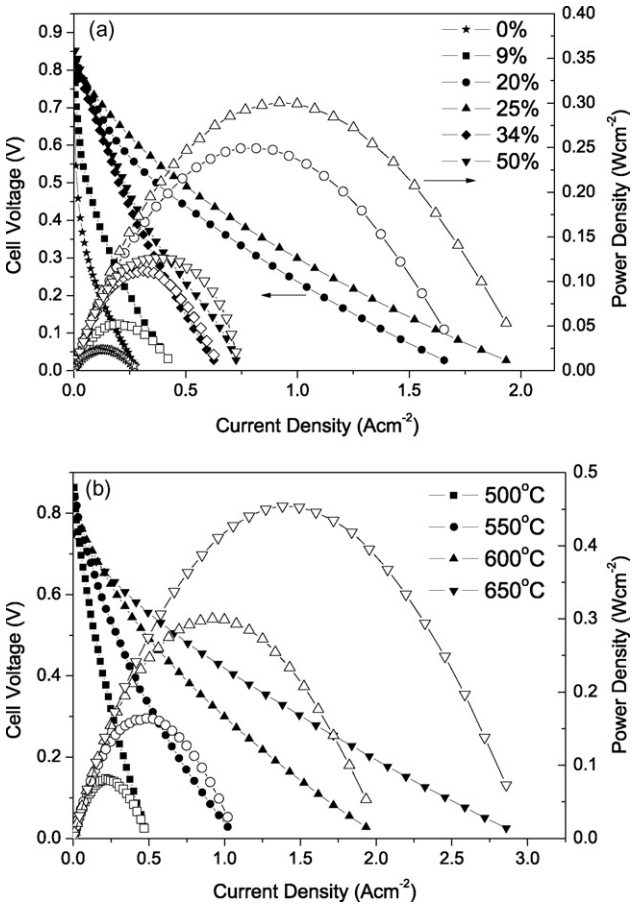

Fig. 9. (a) *V–I* performance measured at 600 °C for anode-supported single cells with LSM cathodes impregnated with various YSB, and (b) cell performance of cell with LSM impregnated with 25% YSB at 500–650 °C.

difference between electrodes with different YSB heating temperatures. So, the heating temperature dependence could be mainly attributed to the microstructure difference. Elevating the heating temperature would coarsen the YSB particles and result in a low specific surface area. Meanwhile, high heating temperature could strengthen the adhesion between the electrode components as well as the electrode and electrolyte. In this study, the latter played a more important role, so the R_p decreased with YSB firing temperature until 800 °C. When YSB was fired at 850 °C, the R_p drastically increased; this is possibly because of severe coarsening of YSB particles as the melting point of Bi_2O_3 is 825 °C [2].

3.5. Stability

The stability of the YSB impregnated LSM electrodes was investigated with 40% YSB impregnated LSM electrode, and the LSM and YSB was fired 900 °C and 800 °C for 2 h, respectively. As shown in Fig. 8, the R_p exhibited 8% perturbation at 700 °C within 200 h and was in the range of 0.154 ± 0.012 Ω cm^2, while that of the Ag-YSB electrodes increased by more than 70% after 100 h at 650 °C [6]. This demonstrates YSB impregnated LSM electrodes were pretty stable for the use in IT-SOFC.

3.6. Single cell performance

The performance of YSB impregnated LSM cathodes was further evaluated with single cells based on SDC electrolytes and Ni-SDC anodes. Shown in Fig. 9a is the cell voltage and power density as

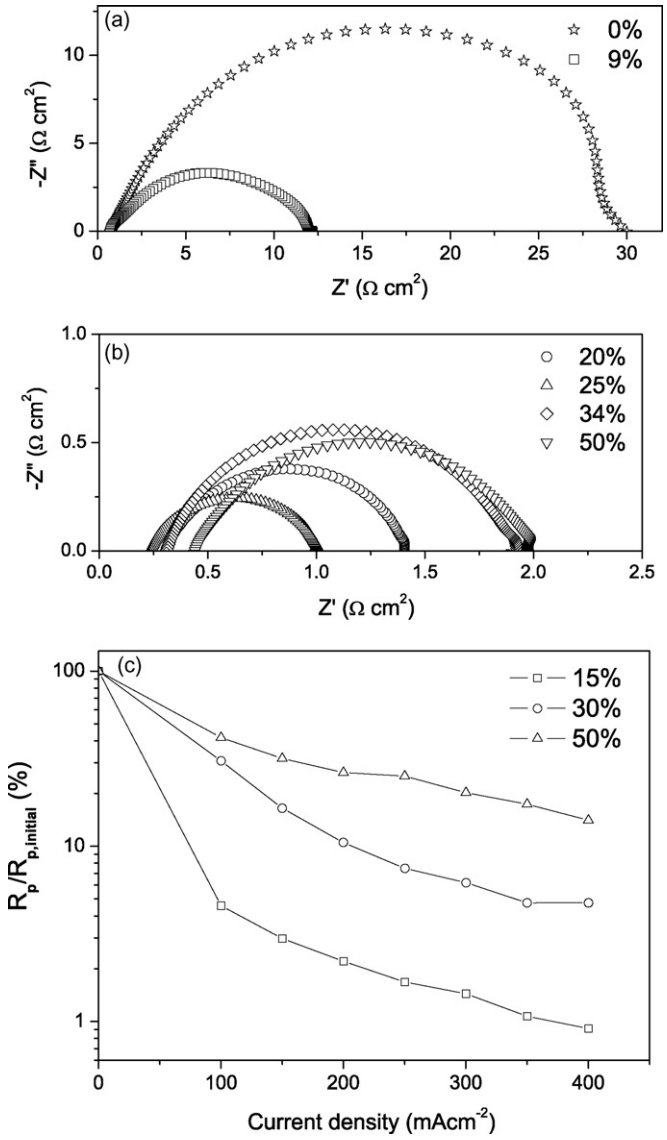

Fig. 10. (a) and (b) Impedance spectroscopy at 600 °C for single cells with various YSB loading measured under open-circuit conditions, and (c) dependence of R_p on cathodic current density. The $R_{p,initial}$ is the polarization resistance measured at open-circuit conditions.

a function of current density for cells with LSM cathodes impregnated with various amounts of YSB at 600 °C. The power density increases with the loading when YSB loading is lower than 25%. The reason for performance improvement by introducing YSB is possibly the same as that for symmetrical cells, which has been discussed above. The cell yielded the maximum power density when LSM had 25% of YSB loading. Cell with YSB loading of 34% and 50% showed much lower power output, which might be due to the concentration polarization loss at decreased porosity of the cathode. Shown in Fig. 9b is the performance at 500–650 °C of a cell with 25% of YSB impregnated LSM cathode. The maximum power densities at 500 °C, 550 °C, 600 °C, and 650 °C were 81 mW cm^{-2}, 164 mW cm^{-2}, 300 mW cm^{-2}, and 454 mW cm^{-2}, respectively. The maximum power density (300 mW cm^{-2}, at 600 °C) is much higher than 138 mW cm^{-2}, the highest power density at 600 °C reported for cells with LSM-based cathodes, and with SDC impregnated LSM cathode [25]. This shows the possibility of the application of LSM-based electrodes to SOFCs operated at temperature as low as 600 °C.

Shown in Fig. 10a and b is the impedance spectra measured under open-circuit conditions. The impedance measurement agrees with the *I–V* test. The lowest polarization resistance was observed when YSB loading was 25%. In addition, the cell with smaller interfacial polarization resistance was obtained with the impedance spectrum showed higher *V–I* performance. But the dependence of polarization resistance on YSB loading obtained with the single cells is quite different to that measured with the symmetrical cells. The lowest interfacial polarization resistance for the single cells was observed with 25% of YSB loading whereas 50% of YSB resulted in the smallest polarization resistance for the symmetrical cells. When 50% of YSB was impregnated, the total interfacial polarization resistance obtained with single cell was 1.53 Ω cm^2, meanwhile the cathodic polarization resistance obtained with the symmetrical cell was 1.08 Ω cm^2. This was reasonable since the total resistance was contributed from both the cathode and anode. However, when 25% of YSB was impregnated, the total resistance measured with the single cell was even smaller than the cathodic resistance measured with the symmetrical cell. The low resistance measured with the single cell is possibly due to the activation process of the cathode when the cell is operated. Although the impedance spectra were measured under open-circuit conditions, actually there was current passing though the cell because of the mixed conducting behavior of the SDC electrolytes [26]. The current passage would activate the cathode and result in much smaller interfacial polarization resistance, which was widely observed with LSM-based electrodes [14,27,28]. To verify this current activation effect on the YSB impregnated LSM electrodes, three-electrode half cells were fabricated with YSB impregnated LSM as working electrodes, and polarization resistance was measured under different current densities. Shown in Fig. 10c is the percentage of R_p measured under the same cathodic current as that measured under open-circuit condition, $R_{p,\,initial}$. The measured R_p decreased when the current density increased, indicating obvious activation effect of current. Furthermore, the activation effect is more obvious when the YSB loading is lower. This could partly explain: (1) why the total polarization resistance of a single cell with low YSB loading is even smaller than the cathodic resistance measured with symmetrical cell, and (2) why the lowest polarization resistance was yielded for a single cell when YSB was 25% other than 50%. In addition to the current effect, when a mixed conductor, doped ceria, is used as the electrolyte, the interfacial polarization resistance of a single cell should not be simply determined by the difference between the real arc intercepts. The interfacial polarization resistance, R_p can be expressed as follows [29]:

$$R_p = \frac{R_T - R_b}{(V_{OC}/E_N)[1-(R_b/R_T)(1-(V_{OC}/E_N))]} \quad (2)$$

where R_T and R_b correspond to the low and high frequency intercept of the impedance arc with the real axis, respectively, V_{OC} is the open-circuit voltage of the cell, and E_N is the Nernst potential across the electrolyte. According to Eq. (2), R_p is always greater than the difference between the low and high frequency intercept, $R_T - R_b$.

4. Conclusions

It has been demonstrated that bismuth oxide was a promising oxygen ion conducting component for LSM-based IT-SOFC cathodes. YSB impregnated LSM cathodes were successfully fabricated on SDC electrolytes. No obvious interaction between YSB and LSM was observed under the IT-SOFC operating conditions. The resulting cathodes showed much smaller area specific polarization resistance than those reported based on LSM. High oxygen ionic conductivity and nanosized particles might be the important rea-

sons for the high performance of the YSB loaded electrode. Single cells with 25% of YSB loading generated a maximum power density of 300 mW cm^{-2} at temperature as low as 600 °C, which shows the possibility of application of LSM-based cathodes operating at low temperatures.

Acknowledgements

This work was supported by the Natural Science Foundation of China (50672096 and 50730002) and the Ministry of Science and Technology of China (2007AA05Z151).

References

[1] E.P. Murray, S.A. Barnett, Solid State Ionics 143 (2001) 265–273.
[2] N.M. Sammes, G.A. Tompsett, H. Näfe, F. Aldinger, J. Eur. Ceram. Soc. 19 (1999) 1801–1826.
[3] T. Takahashi, H. Iwahara, T. Arao, J. Appl. Electrochem. 5 (1975) 187–195.
[4] J.C. Boivin, G. Mairesse, Chem. Mater. 10 (1998) 2870–2888.
[5] C.R. Xia, Y.L. Zhang, M.L. Liu, Appl. Phys. Lett. 82 (2003) 901–903.
[6] M. Camaratta, E. Wachsman, Solid State Ionics 178 (2007) 1242–1247.
[7] H.X. Hu, M.L. Liu, J. Electrochem. Soc. 143 (1996) 859–864.
[8] J.L. Li, S.R. Wang, Z.R. Wang, R.Z. Liu, T.L. Wen, Z.Y. Wen, J. Power Sources 179 (2008) 474–480.
[9] A.F. Poluyan, A.A. Vecher, V.V. Samokhval, A.A. Savitsky, Vestn. Belarus. Univ. Ser. 2 (1984) 5.
[10] T. Hisashige, Y. Yamamura, T. Tsuji, J. Alloys Compd. 408–412 (2006) 1153–1156.
[11] R.D. Purohit, B.P. Sharma, K.T. Pillai, A.K. Tyagi, Mater. Res. Bull. 36 (2001) 2711–2721.
[12] X.Y. Xu, Z.Y. Jiang, X. Fan, C.R. Xia, Solid State Ionics 177 (2006) 2113–2117.
[13] C.R. Xia, M.L. Liu, Solid State Ionics 144 (2001) 249–255.
[14] Y.J. Leng, S.H. Chan, K.A. Khor, S.P. Jiang, J. Solid State Electrochem. 10 (2006) 339–347.
[15] E.P. Murray, T. Tsai, S.A. Barnett, Solid State Ionics 110 (1998) 235–243.
[16] J.D. Kim, G.D. Kim, J.W. Moon, Y. Park, W.H. Lee, K. Kobayashi, M. Nagai, C.E. Kim, Solid State Ionics 243 (2001) 379–389.
[17] M.J.L. Østergård, M. Mogensen, Electrochim. Acta 38 (1993) 2015–2020.
[18] M.J. Jørgensen, M. Mogensen, J. Electrochem. Soc. 148 (2001) A433–A442.
[19] G.B. Jung, T.J. Huang, C.L. Chang, J. Solid State Electrochem. 6 (2002) 225–230.
[20] A.F. Poluyan, Ph.D. Thesis, Belarus State University, Minsk, 1987.
[21] K.Q. Huang, J. Electrochem. Soc. 151 (2004) A716–A719.
[22] N.T. Hart, N.P. Brandon, M.J. Day, N. Lapena-Rey, J. Power Sources 106 (2002) 42–50.
[23] K.C. Wincewicz, J.S. Cooper, J. Power Sources 240 (2005) 280–296.
[24] R.R. Peng, C.R. Xia, Q.X. Fu, G.Y. Meng, D.K. Peng, Mater. Lett. 56 (2002) 1043–1047.
[25] L. Zhang, F. Zhao, R.R. Peng, C.R. Xia, Solid State Ionics 179 (2008) 1553–1556.
[26] M. Mogensen, N.M. Sammes, G.A. Tompsett, Solid State Ionics 129 (2000) 63–94.
[27] S. Mcintosh, S.B. Adler, J.M. Vohs, R.J. Gorte, Electrochem. Solid-State Lett. 7 (2004) A111–A114.
[28] X.J. Chen, K.A. Khor, S.H. Chan, Solid State Ionics 167 (2004) 379–387.
[29] M.L. Liu, H.X. Hu, J. Electrochem. Soc. 143 (1996) L109–L112.